International Journal of Nanomedicine

Dovepress

open access to scientific and medical research

Open Access Full Text Article

ORIGINAL RESEARCH

HA-DOPE-Modified Honokiol-Loaded Liposomes Targeted Therapy for Osteosarcoma

Xiangxiang Zhang, Huaen Chen, Yang Zhang, Qijing Huang, Jianjia Feng, Haoyu Xing, Xiaguo Fu, Xiufang Yan, Yingying Zhang, Qin Xu, Jianming Liang

Artemisinin Research Center, The First Affiliated Hospital, Guangzhou University of Chinese Medicine, Guangzhou, 510405, People's Republic of China

Correspondence: Jianming Liang, Artemisinin Research Center, The First Affiliated Hospital, Guangzhou University of Chinese Medicine, Guangzhou, 510405, People's Republic of China, Email liangjianming@gzucm.edu.cn

Purpose: Osteosarcoma (OS) is the most common bone cancer with a high risk of metastasis, high growth rate, and poor prognosis. Honokiol (HNK) is a general ingredient of traditional Chinese medicine, with a potential anti-tumor effect. However, HNK is insoluble in water and lacks drug targeting, which limits its clinical application. To improve the OS therapeutic effect of HNK, we used HNK-loaded liposomes modified with hyaluronic acid-phospholipid conjugates (HA-DOPE) to treat OS based on the HA interaction with CD44.

Methods: The HNK-loaded liposomes were prepared via thin-film hydration and sonication. HA-DOPE was used to combine the HNK-loaded liposomes (HA-DOPE@Lips/HNK) via sonication and co-extrusion. HA-DOPE@Lips/HNK were characterized with respect to size, zeta potential, polymer dispersity index (PDI), and stability, and transmission electron microscopy was performed. Cellular uptake, cell viability, cell apoptosis, cell cycle, and mitochondrial activity were utilized to evaluate the antitumor effect in vitro. The biodistribution, xenograft tumor growth inhibition, and safety of HA-DOPE@Lips/HNK were evaluated in 143B OS xenograft mice in vivo.

Results: The particle size, PDI, and zeta potential of HA-DOPE@Lips/HNK were 146.20±0.26 nm, 0.20±0.01, and −38.45±0.98 mV, respectively. The encapsulation rate and drug loading were 80.14±0.32% and 3.78±0.09%, respectively. HA-DOPE@Lips/HNK could inhibit cell proliferation, cause apoptosis, block the cell cycle and disrupt mitochondrial activity. HA-DOPE@Lips/HNK specially delivered the drug into the tumor and inhibited tumor growth, and showed no obvious toxicity to normal tissues.

Conclusion: HA-DOPE@Lips/HNK could deliver HNK into the tumor site and had a good antitumor ability in vitro and in vivo. In addition, HA-DOPE@Lips/HNK increased the antitumor effects of HNK. Thus, it provides a promising nanocarrier to improve drug delivery in OS therapy.

Keywords: honokiol, liposomes, osteosarcoma, hyaluronic acid

Introduction

Osteosarcoma (OS) is the most common bone cancer which occurs in children, young people, and sometimes elders.[1] OS seriously threatens patients' lives with a high risk of metastasis, high growth rate, and poor prognosis.[2] The current treatment for OS is mainly surgical resection and chemotherapy.[3,4] In recent years, immunotherapy has been gradually used in the treatment of OS.[5] However, the toxic side effects of chemotherapy drugs have caused many adverse effects on patients, such as cardiotoxicity and nephrotoxicity,[6] and they reduce patients' compliance.[7] Furthermore, the high aggressiveness and poor prognosis increase the difficulty of treatment of OS; therefore, seeking safe and effective treatments for OS is challenging.[8]

In recent years, the development of nanotechnology is bringing hope to patients. Nanotechnology can deliver various drugs to tumors, and some nanomaterials have high loading capacity, and good drug release,[9] while reducing the toxic side effects of chemotherapy drugs.[10] Moreover, some nanomaterials have been designed for targeted treatment of OS

Received: 4 May 2022
Accepted: 31 August 2022
Published: 1 November 2022

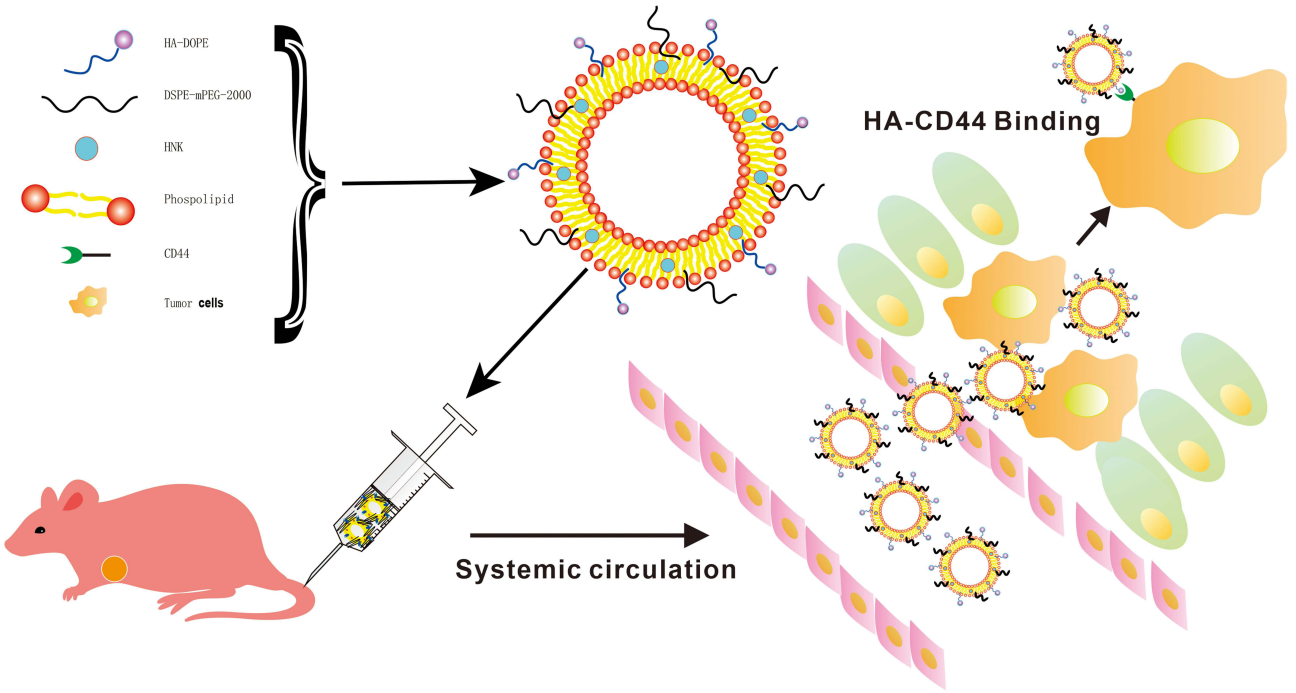

Figure 1 Illustration of the OS targeting treatment strategy of HA-DOPE@Lips/HNK.

based on the overexpression of specific surface receptors in OS cells, the OS tumor environment, or the physiological composition of bones.[11]

CD44 is overexpressed in high levels on the surface of numerous tumor cells; however, it is expressed in low levels on various cell types of normal tissues and the surface of epithelial, hematopoietic, and neuronal cells.[12,13] Hyaluronic acid (HA) is a major component of the extracellular matrix, and it is a naturally occurring glycosaminoglycan that exists in living systems.[14] CD44 is a specific receptor for HA,[15] and HA is utilized to deliver various antitumor drugs to tumors owing to its specific binding affinity with CD44.[16] However, the high hydrophilicity of HA impedes its use in drug delivery. HA has been utilized to modify the micelle for OS targeting and deliver the hydrophobic anticancer drug curcumin with good antitumor activity.[17] Therefore, HA was used to modify the lipid-based nanocarriers to deliver drugs.

Honokiol (HNK) is a small-molecule polyphenol isolated from the genus Magnolia and has antiangiogenic, anti-inflammatory, and antitumor activities. The antitumor effect of HNK has been extensively researched.[18] However, the insolubility of HNK in water limits its clinical applications. Nanotechnology, which can be used to encapsulate insoluble drugs through liposomes, polymers, and nanoparticles, can be used to improve the aqueous solubility and bioavailability of HNK.[19–21]

In this study, HA was linked to DOPE by an ester bond to form HA-DOPE, which was utilized to modify liposomes loaded with HNK (HA-DOPE@Lips/HNK) (Figure 1). HA-DOPE@Lips/HNK could deliver HNK to the OS site and target $CD44^+$ OS cells and improve the antitumor effect of HNK with high biocompatibility. Thus, it is a promising strategy for the treatment of OS.

Materials and Methods

Chemicals and Reagents

Soybean phospholipids (SPC) and the DOPE were AVT Pharmaceutical Technology Co., Ltd. (Shanghai, China). The DSPE-mPEG2000 was the product of HuaTeng Pharma (Hunan, China). HA (molecular weight (MW=10 kDa) was offered by Liyoung Biotechnology Co., (Shandong, China). HNK was supplied by Meilunbio (Dalian, China). Hoechst 3342 (HO), propidium Iodide (PI), 4-Dimethylaminopyridine (DMAP), 1-ethyl-(3-dimethylamino-propyl) carbodiimide hydrochloride (EDC), cholesterol (CHO) and N-Hydroxysuccinimide (NHS) were purchased from Damas-beta

(Shanghai, China). Fetal bovine serum (FBS), RPMI1640, 3-(4,5-dimethyl-thiazol-2-yl)-2,5-diphenyl-*tetra*-zolium bromide (MTT), Annexin V-Cy5 was purchased from Thermo Fisher scientific. The anti-CD44, goat Anti-rabbit IgG H&L/Cy3 were offered by Bioss (Beijing, China). The 143B cell and MCF-7 cell were purchased from Cell Bank of the Chinese Academy of Sciences (Shanghai, China).

Synthesis of HA-Linked DOPE

HA-DOPE conjugation was synthesized by a modified reaction.[22] Briefly, 10mg HA was dissolved in 1mL H_2O and observed the HA completely dissolved, added 1mg DMAP into the HA solution, then used 0.1M HCl to adjust the solution to pH 5.0, subsequently added 120mg EDC, 120mg NHS into the reaction solution. Similarly, the pH was adjusted to 5.0 with the 0.1M HCl and the whole reaction solution activated at room temperature for 4h. Next, the DOPE was dissolved in 1mL tetrahydrofuran, added it into the whole reaction slowly, maintained the pH at 5.0 in the whole reaction solution for 24h at room temperature. After reaction, the pH was adjusted to 7.0 with 0.1 M NaOH, the whole reaction solution through rotary evaporation to remove the excess tetrahydrofuran, the reaction solution was purified by a cellulose membrane (MW=14 kDa) and dialyzed for 48h, the HA-DOPE was finally obtained by freeze-drying. HA-DOPE was identified by a Fourier transformation infrared spectrometer (FT-IR, R330) and high-performance liquid chromatography (HPLC).

Preparation of the HNK-Loaded Liposomes

The HNK-loaded liposomes (Lips/HNK) was prepared using combined methods of thin-film hydration and sonication. In briefly, soybean phospholipids (SPC), cholesterol, DSPE-mPEG2000, HNK was at a quality ratio of 10:3.5:2:1, and those materials were dissolved into chloroform and methanol at a volume ratio of 1:4. The solution was dried using the rotary evaporator to form the thin-film of the HNK loaded, the film was hydrated using the 2mL 5% glucose solution and was sonicated using the probe sonicator for 10 min at 150W, and the loaded HNK solution was filter through a 0.22-μm microfiltration membrane.

Preparation the HA-DOPE Modify the HNK-Loaded Liposomes

The HA-DOPE-modified HNK-loaded liposomes (HA-DOPE@Lips/HNK) were prepared using combined methods of sonication and co-extrusion method. Briefly, the hydrophobic part of HA-DOPE is inserted into the phospholipid bilayer of liposomes, the quality ratio of HA-DOPE: Lips/HNK was 1:5, and the solution was through 200nm polycarbonate filters (Avestin, Ottawa, Canada), using a small volume extrusion apparatus (LiposoFast tm Basic, Avestin). The thus-formed liposomes were HA-DOPE@Lips/HNK.

Characterization of the HA-DOPE@Lips/HNK

The particles sizes, polymer dispersity index (PDI) and the zeta potential of the HA-DOPE@Lips/HNK were measured by the Zetasizer nano-ZS90 instrument, and the morphology of the HA-DOPE@Lips/HNK was observed by the transmission electron microscopy (TEM). The stability of the HA-DOPE@Lips/HNK is measured by the nano-ZS90, including the particle size change for 7 days at 4°C in PBS and for 24h at 37°C in 10% FBS. Infra-red spectroscopy analyses of HNK, blank liposomes, physical mixture (SPC, CHO, DSPE-mPEG2000, HA-DOPE and HNK) and HNK-loaded liposomes (HA-DOPE@Lips/HNK) were performed using a Fourier transform infrared spectrophotometer (FT-IR).

High-Performance Liquid Chromatography Method for Assaying the HNK

The HNK concentration was measured by the HPLC (Agilent, USA), C18 column was used for the in vitro and in vivo detection of the HNK, and the composition of the mobile phase was methanol: water (75:25, v/v), with the flow rate was 1.0mL/min, and the detection wavelength was 294nm, the C18 Column temperature was set at 25°C, and the limits of detection and quantitation were 15.625 and 500μg/mL.

The Entrapment Efficiency and the Drug Loading

The encapsulation efficiency and drug loading of liposomes were determined by HPLC. For the determination of encapsulation efficiency, the liposomes was diluted with methanol (1:9, v/v), the solution was shaken for 5 min to

broke the liposomes structure, and centrifuged at 15,000 rpm for 10 min, the solution was filtered with a 0.22-μm microfiltration membrane, and the honokiol concentration was analyzed by the HPLC methods. For the measured the drug loading, the liposomes were freeze-dried and resuspended and dissoloved in water, the solution was sonicated and filtered with the 0.22-μm microfiltration membrane, and the honokiol was analyzed by the HPLC.

Cell Uptake Assay

Cell culture: human bone osteosarcoma (143B) cells were cultured in RPMI1640 which contained the 10% fetal bovine serum and 1% penicillin–streptomycin at 37°C in a 5% CO_2 incubator.

The 143B cells were seeded into the 6-well plates at a density of 3×10^5 cells per well and the cells were cultured overnight at 37°C in a 5% CO_2 incubator; the liposomes were labelled with the coumarin 6 (C6); the liposomes and the HA-DOPE@Lips were added to each well with the same fluorescence intensity, respectively; the liposomes was incubated with the cells for 2h; then the cells were rinsed with PBS for 3 times; finally, each well cell was collected and resuspended in 300μL PBS, and the fluorescence intensity of the each well was measured useing flow cytometry (Cyto FLEX, USA).

For upright fluorescence Microscopy (Olympus, Japan), 143B cells were seeded into the 24-well plates at a density of 5×10^4 cells per well and the cells were cultured overnight at 37°C in a 5% CO_2 incubator, as described previously; the liposomes were labelled with the C6 and incubated with the cells for 2h; the liposomes were discarded and added the Hoechst 3342 (HO) into the cells incubated 15 min; and then discarded the HO solution and the cells were rinsed PBS for 3 times. Finally, the cell slides were mounted with the glycerol/gelatin jelly sealing reagent, and observed by the fluorescence microscopy.

Cell Viability Assay

The cell viability of 143B cells assay was evaluated by MTT assay. Briefly, 143B cells were seeded into the 96-well plates at a density of 8×10^3 cells per well, the cells were incubated for 24h; 100μL of the HNK, Lips/HNK, HA-DOPE @Lips/HNK solution were added and incubated with the cells for 48h; then, per plates were added the 10μL MTT (5mg/mL) and cultured in the incubator for 4h; the solution was discarded; the per plates were added the 100μL dimethyl sulfoxide (DMSO). The absorbance intensity of each well was measured at the 490 nm, and the IC50 values were calculated and compared.

Apoptosis Assay

For flow cytometry, 143B cells were seeded into 6-well plates at a density of 3×10^5 cells per well, cultured overnight. The cells were treated with HNK, Lips/HNK, HA-DOPE@Lips/HNKwith the same concentration for 48h, then the cells were stained with the Annexin Ⅴ-Cy5/PI for 0.5h and detected by flow cytometry.

For upright fluorescence microscopy, 143B cells were seeded into the 24-well plates at a density of 5×10^4 cells per well. The cells were treated with HNK, Lips/HNK, HA-DOPE@Lips/HNK for 24h. Then, the cells stained with HO and PI solution for 0.5h. Finally, the cell slides were mounted with the glycerol/gelatin jelly sealing reagent, and observed by the fluorescence microscopy.

Cell Cycle Assay

Logarithmic growth phase of 143B cells was seeded into the 6-well plates and cultured 24h. The cells were treated with HNK, Lips/HNK, HA-DOPE@Lips/HNK with the same concentration for 24h. After being washed for 3 times, the cells were collected, and fixed in cold ethanol at −20°C for overnight. Then, the cells were washed for 3 times and treated with the PI and RNA polymerase solution (50μg/mL) for 0.5h, and finally detected by flow cytometry.

Mitochondrial Activity Assay

Logarithmic growth phase of 143B cells was seeded into the 6-well plates and cultured overnight; the cells were treated with HNK, Lips/HNK, HA-DOPE@Lips/HNK with the same concentration for 24h. Then, the cells were stained with

Mito Tacker ™ Deep Red FM for 0.5h. After being washed for 3 times, the cells were collected and resuspended in 300μL PBS and measured by flow cytometry.

Expression Level of CD44 in 143B Cell

As previously mentioned, 143B and MCF-7 cells were seeded into 6-well plates and cultured overnight. The cells were treated with the primary antibody of CD44 for 2h at 4°C, then the primary antibody were discarded, and the cells were rinsed with PBS for 2 times, next the second antibody goat anti-rabbit IgG H&L/Cy3 was added to the cells. After the cells were incubated for 1 h at 4°C, the second antibody was discarded and rinsed with PBS for 3 times, and the cells were resuspended in 300μL PBS and measured by the flow cytometry.

The Liposomes and CD44 Co-Localization in Cells

Logarithmic growth phase of 143B cells was seeded on the cell slide and cultured overnight, HA-DOPE@Lips was labelled with the DiD. The cells were co-incubated with HA-DOPE@Lips/DiD for 2h, then rinsed with PBS for 3 times. After 2h incubation with the primary antibody of CD44 at 37°C, the cells were rinsed with PBS 3 times and incubated with second antibody goat anti-rabbit IgG H&L/Cy3 at 4°C for 1h, then the HO solution added into the cells for 20 min. Finally, the cells were rinsed with PBS 3 times, mounted with the glycerol/gelatin jelly sealing reagent and observed by the laser scanning confocal microscopy.

HA Inhibited the Cell Uptake

Logarithmic growth phase of 143B cells was seeded into 6-well plates and cultured overnight. The cells were treated with free HA (1000, 500, 250, 125, 62.5, 32.25μg/mL) for 2h, then HA-DOPE@Lips/DiD was added to the cells for 2h. Next, the solution was discarded and the cells were rinsed with PBS for 3 times. Finally, the cells were resuspended in 300μL PBS and measured by flow cytometry.

Biodistribution in vivo

The Lips and HA-DOPE@Lips biodistribution in vivo was observed using the living imaging system (VIEWORKS, Korea), and the liposomes were labelled with the DiD. The tumor-bearing nude mice were injected with the same fluorescence intensity of the Lips/DiD and the HA-DOPE@Lips/DiD via the tail vein, the tumor-bearing nude mice were observed the 1, 2, 4, 6, 8h by the living imagine system. Then the mice were sacrificed and tumors and the major organs were harvested, the tumors and organs respectively were observed by the living imagine system. The tumors were harvested and Lips/DiD and HA-DOPE@Lips/DiD distribution were observed in the tumor. Briefly, the tumor samples were embedded and frozen in the OCT compound and cut into 10μm thick sections, stained with anti-CD44 monoclonal antibodies at 1:100 for overnight, then stained with goat anti-rabbit IgG H&L/Cy3 for 2h. Finally, the sections were stained with HO and observed by laser scanning confocal microscopy.

In vivo Antitumor Assay

The nude mice xenograft model of OS was established by the subcutaneous injection of 5×10^6 143B cells into the left forelimb axillae. After the tumor volume reached about 100–150mm^3, the nude mice were divided into four groups, and treated with PBS, HNK (10mg/kg), Lips/HNK (10mg/kg), HA-DOPE@Lips/HNK (10mg/kg) and were injected into the tail vein for 10 times with an interval of 2 days. When the administration time, the tumor of the length diameter and the width diameter were measured, tumor volume=length×1/2 $width^2$, similarly, the body weight was recorded as well. The mice were sacrificed when the second day of the last tail vein injection, the tumors and the major organs were collected, weighted and stored in 4% paraformaldehyde. The major organs were cut into slices, stained with the hematoxylin and eosin (H&E). Tumors were cut into slices, stained with the terminal deoxynucleotidyl transferase-mediated dUTP nick end-labeling (TUNEL). All animals were housed in the Department of Experimental Animal, Guangzhou University of Chinese Medicine Science and Technology Park Co., Ltd (GUCM). All animal studies were conducted in compliance with guidelines evaluated and approved by the ethics committee of GUCM.

Statistical Analysis

The data were analysed using the Prism 7, the data were presented as mean values ±SD, the comparison of the data was using the Student's test and the one-way ANOVA, the P value<0.05 was considered statistically significant.

Results

Synthesis and Characterization of the HA-DOPE

HA-DOPE was synthesized via an amide bond was inserted into the phospholipid bilayer. Meanwhile, HA-DOPE was identified via Fourier-transformation infrared spectroscopy (Figure S1). The characteristic absorption peak of the hydroxyl group in HA was at 3278.71cm^{-1}, the DOPE characteristic absorption peak of the long-chain methylene was at 2918.44 cm^{-1} and 1461.95 cm^{-1}, and the DOPE characteristic absorption peak of the carbonyl group in the ester bond was at 1376.23 cm^{-1}. The HA-DOPE characteristic absorption peaks at 3284.37 cm^{-1} and 1735.63 cm^{-1} indicated the hydroxyl and carbonyl groups in the ester bond of HA and DOPE, respectively. HA and HA-DOPE were identified via HPLC (Figure S2). A BioCore SEC column (size-exclusion chromatography column) was used for identifying HA-conjugated DOPE. The retention time of the sample is related to its molecular weight: the larger the molecular weight, the shorter the retention time. When HA conjugated to DOPE to form HA-DOPE, the retention time was shorter because of the larger molecular weight. The retention times of HA and HA-DOPE were 5.3 min and 5.1 min, respectively. The above results showed that the HA-DOPE synthesis was successful.

Characterization of the HA-DOPE@Lips/HNK

HA-DOPE@Lips/HNK was prepared via the sonication and co-extrusion method. The particle sizes, PDI, zeta potentials of Lips/HNK and HA-DOPE@Lips/HNK were measured via dynamic light scattering, the morphology of HA-DOPE@Lips/HNK was observed via TEM, and the encapsulation efficiency and drug loading of liposomes were determined via HPLC. The size distribution and zeta potential distribution of HA-DOPE@Lips/HNK are shown in the Figure 2A and 2B. The sizes of the Lips/HNK and HA-DOPE@Lips/HNK were 115.2±0.27nm and 146.2±0.62 nm, respectively (Table 1). The size distribution of Lips/HNK and HA-DOPE@Lips/HNK exhibited good stability with minor size changes in 7 days and even incubated in 10% FBS at 37°C for 24 h (Figure 2C and D). The morphology of HA-DOPE@Lips/HNK showed a spherical shape (Figure 2E). Owing to the HA-DOPE modification, HA-DOPE@Lips/HNK was larger than Lips/HNK. Furthermore, the zeta potential of HA-DOPE@Lips/HNK was more negative than that of Lips/HNK, which should be caused by the carboxyl groups of HA. The encapsulation efficiency and drug loading of Lips/HNK were approximately 82.96±0.94% and 4.84±0.06%, respectively, whereas those of HA-DOPE@Lips/HNK were approximately 80.14±0.32% and 3.78±0.09 (Table 1).

FT-IR spectrophotometry was used to assess the encapsulation of HNK in liposomes. The FT-IR spectra of pure HNK, blank liposomes, physical mixture (SPC, CHO, HA-DOPE and HNK) and HA-DOPE@Lips/HNK are shown in Figure S3. In the HNK spectrum (Figure S3A), a strong peak at 3000–3300 cm^{-1} corresponded to the vibration of the –CH and –OH bonds. The absorption peak at 1639 cm^{-1} was attributed to the stretching vibration of the C=C group, and the peaks at 1493 cm^{-1} and 1428 cm^{-1} were characteristic signals of the stretching vibration of the benzene ring skeleton in HNK. What's more, the bands centered at 1208 cm^{-1} and 907 cm^{-1} were assigned to C–O vibration. As described in the spectrum of blank liposomes (Figure S3B), a broad peak centered at 3284 cm^{-1} corresponded to the O– stretching (HA-DOPE and CHO). The peak at around 1735 cm^{-1} characterizes the C=O stretch of the ester bond (HA-DOPE and SPC). The bands located at 2921 cm^{-1} and 2852 cm^{-1} were characteristic signals of the stretching vibration of the C-H group in SPC and DSPE-mPEG2000. The FT-IR spectrum of the physical mixture (Figure S3C) could be considered as the superposition of Figure S3A and S3B. The spectrum of HA-DOPE @Lips/HNK (Figure S3D) had less intense absorption bands at 1700–1300 cm^{-1} than those of HNK and the physical mixture. The results indicated that HNK was loaded into the liposomes.

Cell Uptake Assay

The cell uptake of 143B cells was measured via flow cytometry and upright fluorescence microscopy (Figure 3A). Lips and HA-DOPE@Lips were labeled with Coumarin 6 (C6). The fluorescence intensity of C6 represented the 143B cells

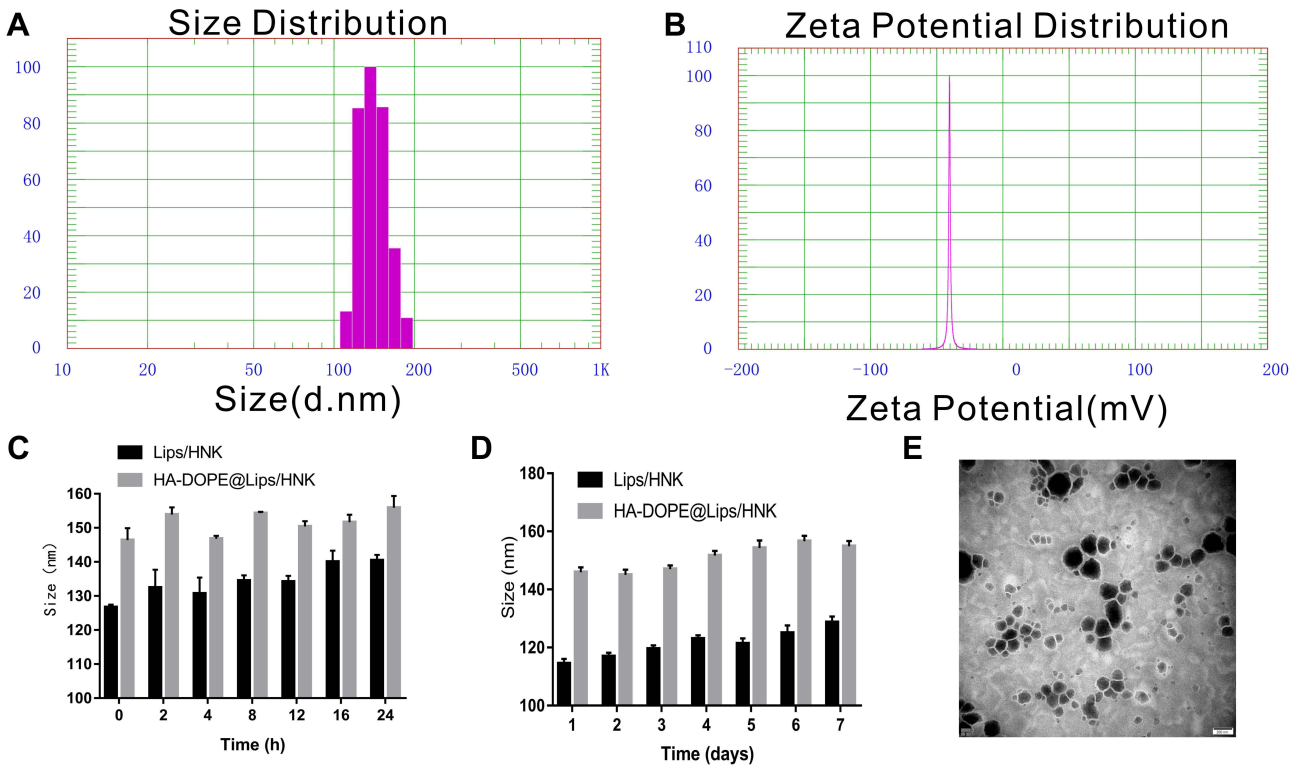

Figure 2 Size distribution of HA-DOPE@Lips/HNK (**A**); zeta potentials distribution of HA-DOPE@Lips/HNK (**B**); size of Lips/HNK and HA-DOPE@Lips/HNK range at 37°C in 10% FBS (**C**); size of the Lips/HNK and HA-DOPE@Lips/HNK range at 4°C in PBS (**D**); TEM image of HA-DOPE@Lips/HNK (**E**).

uptake efficiently. The fluorescence intensity of HA-DOPE@Lips/C6 group was much stronger than that of Lips/C6 group. It indicated that the uptake of HA-DOPE@Lips/C6 was more efficient than that of Lips/C6, which was attributed to endocytosis mediated by the CD44 receptor of the 143B cells. Similarly, the cellular uptake of the nanoparticles of 143B cells was quantitatively measured via flow cytometry (Figure 3B), and the results showed that the HA-DOPE @Lips/C6 group had higher fluorescence intensity than that of the Lips/C6 group, which was consistent with the upright fluorescence microscopy results and indicated the targeting ability of HA-DOPE@Lips.

Table 1 The Characterization of the HA-DOPE@Lips/HNK

	Lips/HNK	HA-DOPE@Lips/HNK
Particle size (nm)	115.2±0.27	146.2±0.62
PDI	0.302±0.03	0.20±0.01
Zeta potential (mV)	−23.79±0.51	−38.45±0.98
Encapsulation efficiency (%)	82.96±0.94	80.14±0.32
Drug loading (%)	4.84±0.06	3.78±0.09

Note: Dates are Shown as Mean±SD (n=3).

Abbreviations: OS, osteosarcoma; HNK, honokiol; HA-DOPE, hyaluronic acid-phospholipid conjugated; PDI, polymer dispersity index; HA, hyaluronic acid; SPC, soybean phospholipids; HO, Hoechst 3342; PI, propidium Iodide; DMAP, 4-Dimethylaminopyridine; EDC, 1-ethyl-(3-dimethylamino-propyl) carbodiimide hydrochloride; NHS, *N*-hydroxysuccinimide; FBS, fetal bovine serum; MTT, 3-(4,5-dimethylthiazol-2-yl)-2,5-diphenyl-*tetra*-zolium bromide; TEM, transmission electron microscopy; HPLC, high-performance liquid chromatography; HE, hematoxylin and eosin; TUNEL, terminal deoxynucleotidyl transferase-mediated dUTP nick end-labeling.

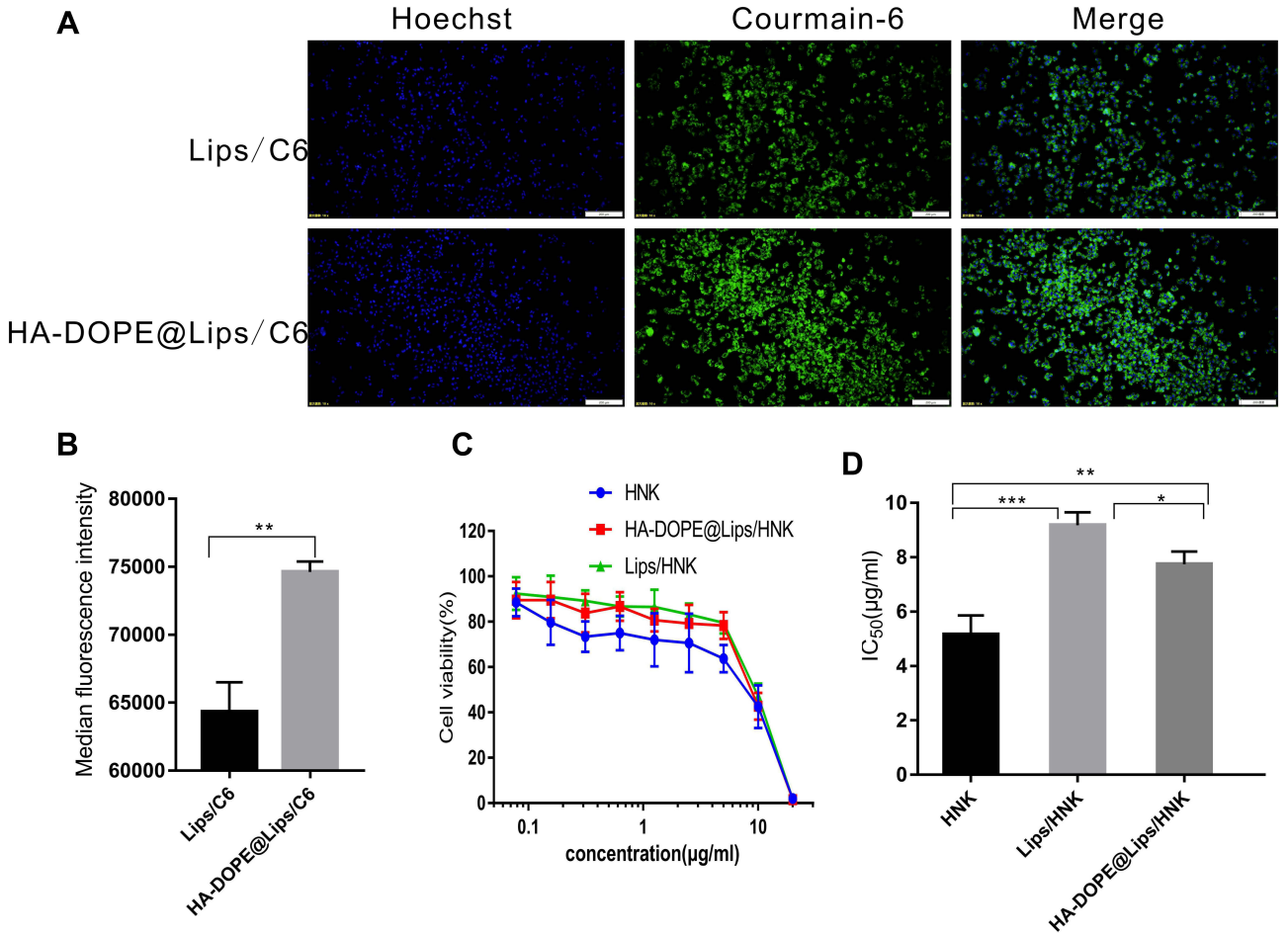

Figure 3 Fluorescence microscopy images of 143B cells (**A**); fluorescence intensity measured via flow cytometry (n=3) (**B**); in vitro cytotoxicity of HNK, Lips/HNK, HA-DOPE@Lips/HNK against 143B cells (**C**); IC_{50} value of HNK, Lips/HNK, and HA-DOPE@Lips/HNK (**D**). Data are presented as mean±SD, (n=6), and *, **, *** represent p values <0.05, <0.01, and <0.001, respectively; the bar is 200 μm.

Immunofluorescence of CD44 Protein in 143B Cell

The CD44 expression level of 143B cells was determined via flow cytometry. As shown in Figure 4B, 143B cells had higher fluorescence intensity than MCF-7 cells (negative control), and 143B cells over-expressed CD44, which can serve as a specific delivery target for 143B cells.

Liposomes and CD44 Co-Localization in Cells

The co-localization of HA-DOEP@Lips/DiD and CD44 in cells was determined via laser scanning confocal microscopy (Figure 4A). HA-DOPE@Lips/DiD showed red fluorescence on the surface of the cells, and CD44 expressed on the surface of the 143B cells showed green fluorescence; the merged image showed yellow fluorescence, which indicated that HA-DOEP@Lips/DiD interacted with CD44 expressed on the surface of 143B cells.

HA Inhibited Cell Uptake

The cellular uptake inhibition by free HA was tested via flow cytometry (Figure 4C). Different concentrations of free HA could inhibit cellular uptake, and the cellular uptake was associated with the interaction between HA and CD44, which is involved in mediating the endocytosis of HA-DOPE@Lips/DiD.

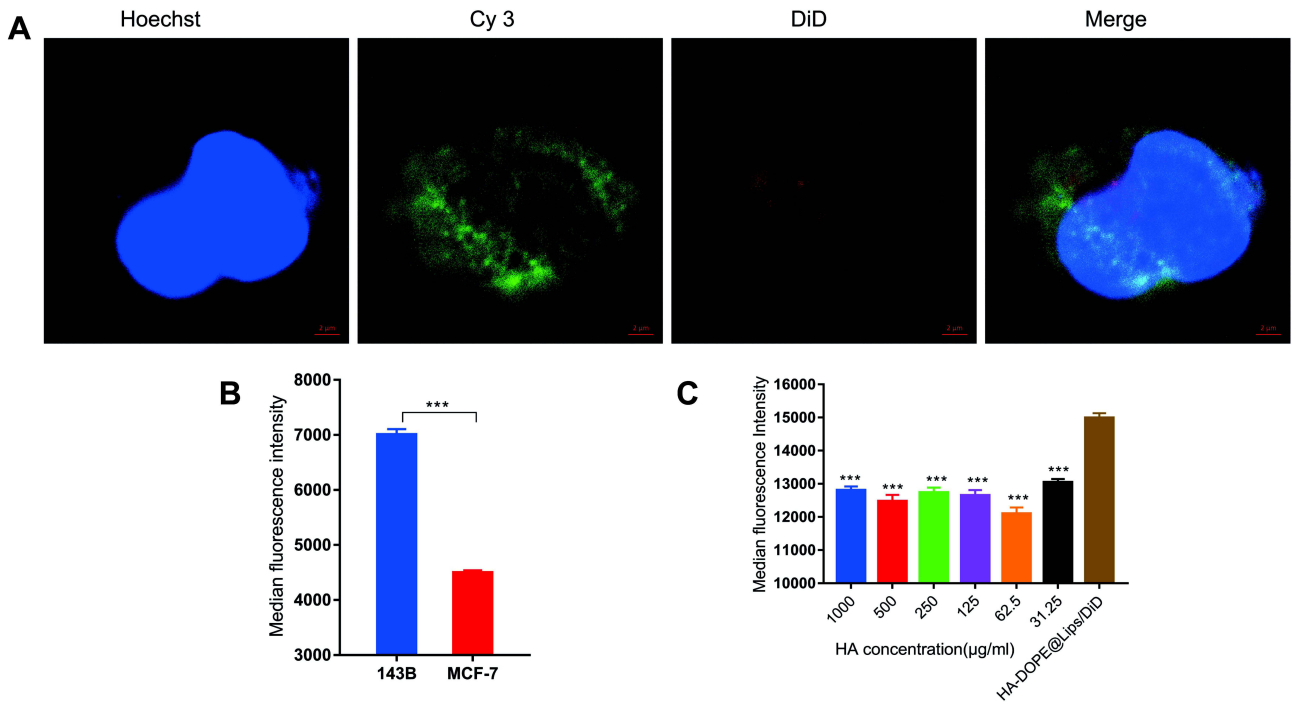

Figure 4 Co-location of HA-DOPE@Lips/DiD and CD44 (**A**); median fluorescence intensity of CD44 stained with Cy3 of 143B and MCF-7 cells (**B**); different concentrations of HA inhibited cell uptake (**C**). Data are presented as mean±SD (n=3), and *** represent p values <0.001; the bar is 2 μm.

Cell Viability Assay

The cell viability of 143B cells was evaluated via an MTT assay, and the results are presented in Figure 3C and D. All drugs (HNK, Lips/HNK, and HA-DOPE@Lips/HNK) reduced cell viability in a dose-dependent manner. The IC_{50} of HNK, Lips/HNK, HA-DOPE@Lips/HNK were 5.16±0.7, 9.18±0.47, and 7.75±0.47 μg/mL, respectively. HA-DOPE@Lips/HNK had higher cytotoxicity than Lips/HNK in 143B cells, which could be attributed to the affinity of HA to CD44 receptor.

Apoptosis Assay

For the apoptosis assay, 143B cells were stained with Annexin V-Cy5/PI using flow cytometry and upright fluorescence microscopy. As shown in Figure 5A and C, HA-DOPE@Lips/HNK induced a higher cell apoptosis ratio than HNK and Lips/HNK. Similarly, as shown in Figure 5F, the red fluorescence intensity of the HA-DOPE@Lips/HNK group was higher than that of any other group. The higher red fluorescence intensity represents the more cell apoptosis with decreasing cell membrane integrity; this is consistent with the flow cytometry results and indicated the apoptotic ability of HA-DOPE@Lips/HNK.

Cell Cycle

The nuclei of 143B cells were stained with PI and determined via flow cytometry. The cell cycle distribution was defined based on the difference in PI fluorescence intensity. As observed in Figure 5B and D, HNK, Lips/HNK and especially HA-DOEP@Lips/HNK could arrest the cell cycle in the G1 phase. In contrast, all drugs decreased the number of cells in the S phase, and the G2/M phase was insignificant in 143B cells after the treatment.

Mitochondrial Activity Assay

The mitochondrial activity of 143B cells was tested using Mito Tacker ^{TM} Deep Red FM Dye. As shown in Figure 5E, the fluorescence intensity represents the cell's mitochondrial activity; when the mitochondria are destroyed, the fluorescence intensity is reduced. HNK, Lips/HNK, and HA-DOPE@Lips/HNK decreased the fluorescence intensity compared to PBS. HA-DOPE@Lips/HNK decreased the mitochondrial activity more efficiently than the other drugs.

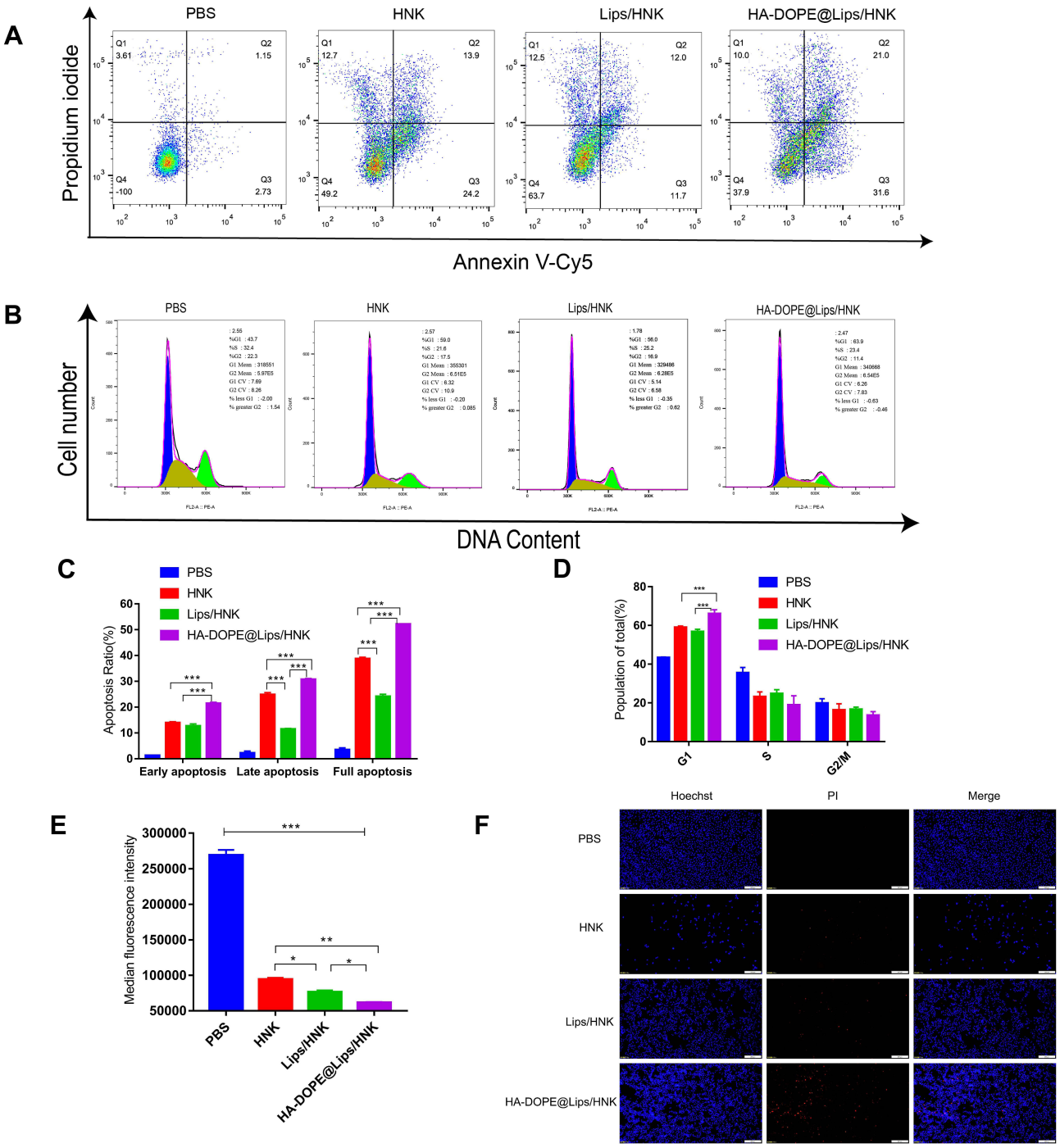

Figure 5 Representative scatter plots of Annexin V-Cy5/PI of 143B cells treated with different drugs (**A**); representative cell cycle distribution of cells after treatment (**B**); apoptosis ratio of the different groups (**C**); population of the different groups in the cell cycle (**D**); fluorescence intensity of mitochondrial labelled with Mito Tacker™ Deep Red FM Dye (**E**), and the fluorescence microscopy images of the different groups in cell apoptosis assay (**F**). Data are presented as mean±SD (n=3), and *, **, *** represent p values<0.05, <0.01, and <0.001, respectively; the bar is 200μm.

Biodistribution in vivo

The in vivo biodistribution of liposomes was observed using a live imaging system, and the liposomes were labeled with DiD. Tumor-bearing mice were administered the same fluorescence intensity of Lips/DiD and HA-DOPE @Lips/DiD via tail vein injection, and we obtained images 1h,2h,4h,6h, and 8h after administration. Then, the tumors and major organs were collected and images were obtained. Figure 6A–C showed that HA-DOPE@Lips/DiD

was accumulated in the tumor; in contrast, Lips/DiD rarely accumulated in the tumor. The tumor fluorescence intensity of HA-DOPE@Lips/DiD was higher than that of Lips/DiD. Furthermore, the results indicated targeting of HA-DOPE@Lips/DiD owing to the interaction of the HA and the CD44. Lips/DiD and HA-DOPE@Lips/DiD were majorly distributed in the liver, lung, and kidneys, rarely distributed in the spleen, heart, and brain (Figure 6D). As shown in Figure 6E, the intensity of red fluorescence represented accumulation of Lips/DiD and HA-DOPE@Lips/DiD in the tumor site; HA-DOPE@Lips/DiD was more accumulated in the tumor site than Lips/DiD. Green fluorescence represented CD44 labeled with Cy3. The tumor slices of Lips/DiD and HA-DOPE@Lips/DiD showed the same fluorescence intensity, which indicated the same CD44 levels. In the merged image, HA-DOPE@Lips/DiD showed pink fluorescence by overlaying the images of green and red fluorescence. This indicated the ability to deliver the drug to the tumor.

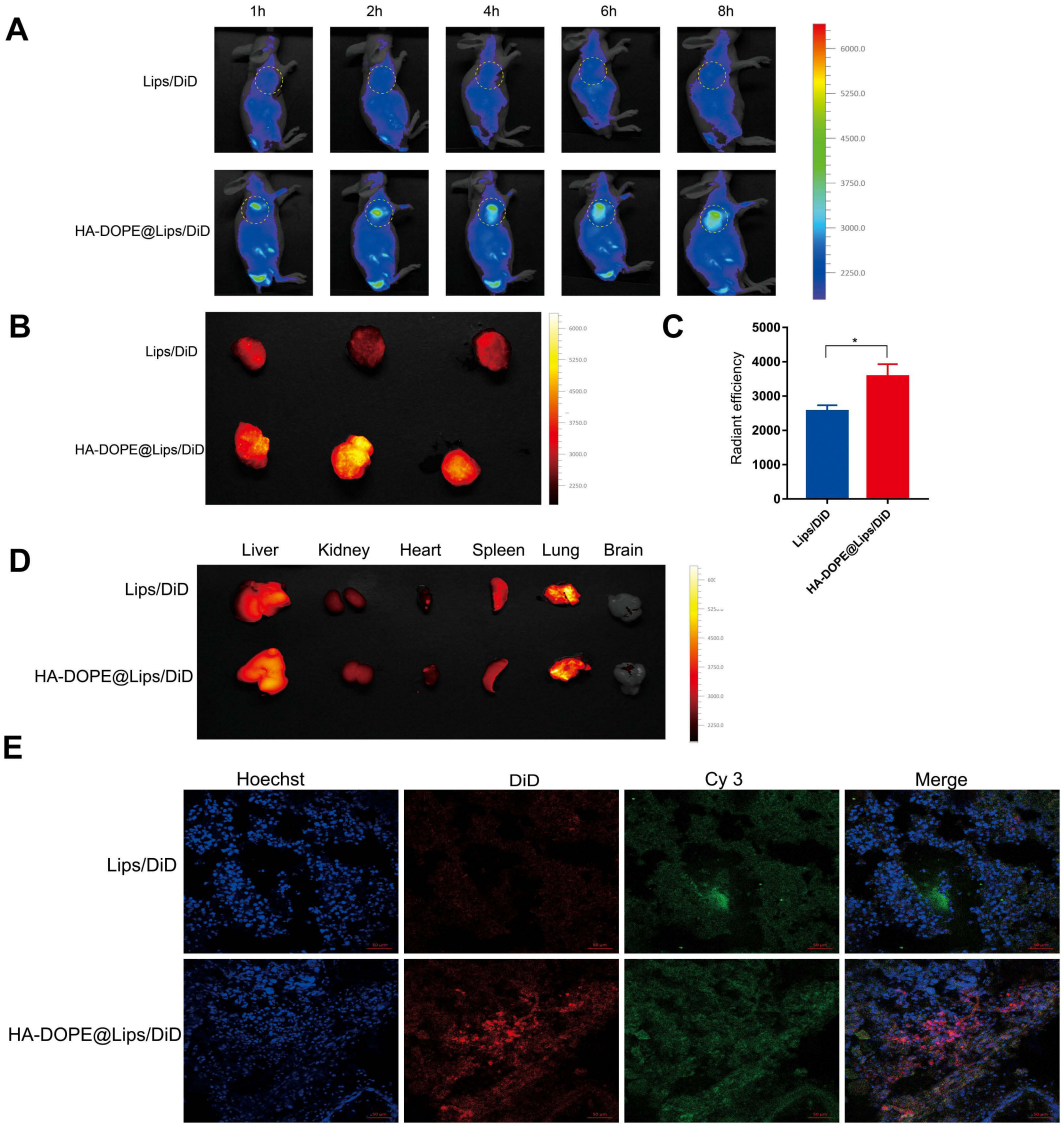

Figure 6 In vivo biodistribution of Lips/DiD and HA-DOPE@Lips/DiD (**A**); Lips/DiD and HA-DOPE@Lips/DiD images of the tumors (**B**); fluorescence intensity of the tumor (**C**); in vivo image of the major organs (**D**); and immunofluorescence images of the tumors (**E**). Data are presented as mean±SD (n=3), and *represent p values<0.05; the bar is 200 μm.

In vivo Antitumor Activity

To assess the antitumor activity of HA-DOPE@Lips/HNK, we performed the in vivo antitumor experiment using OS (143B cells) xenograft models. When the tumor volumes reached 100–150 mm^3, the mice were divided into PBS, HNK, Lips/HNK and the HA-DOPE@Lips/HNK groups. The dose of the HNK concentration was 10mg/kg administered via tail vein, and the mice were treated with the four groups intravenously ten times at an interval of 2 days. As shown in Figure 7A and B, the volume of solid tumors in the PBS group increased in a time-dependent manner; all treatment groups showed significantly repressed tumor growth. The tumor volume of the HA-DOPE@Lips/HNK group was significantly lower than that of the other groups. The tumor weight (Figure 7E) also indicated improved antitumor efficiency of HA-DOPE@Lips/HNK compared to that of HNK and Lips/HNK. These results showed that HA-DOPE@Lips/HNK had good antitumor activity owing to the HA interaction the CD44. The change in the body weight and organ index reflects the drug safety in vivo. As shown

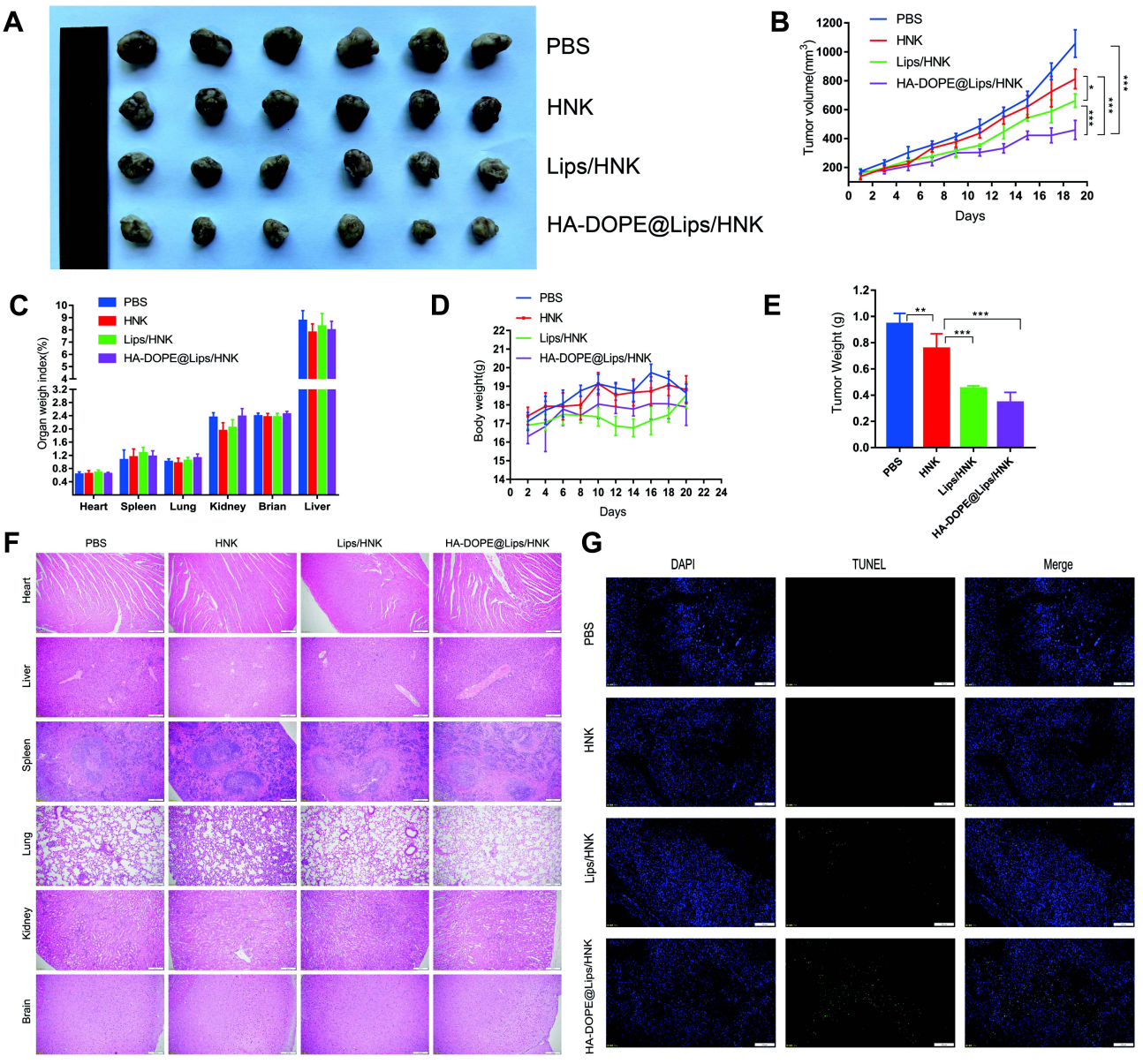

Figure 7 Excised tumors at the end of the experiment (**A**); tumor growth curve in mice during the experimental period (**B**); major organs weigh index (**C**); body weight changes in 143B-bearing nude mice treated with PBS, HNK, Lips/HNK, and HA-DOPE@Lips/HNK (**D**); tumor weight at the end of experiment (**E**); H&E-stained organ slices from 143B-bearing nude mice treated with different formulations after 20 days (**F**); TUNEL images of the tumors (**G**). Data are presented as mean±SD (n=6), and *, **, *** represent p values <0.05, <0.01, and <0.001, respectively; the bar is 200 μm.

in Figure 7C and D, HA-DOPE@Lips/HNK showed no obvious body weight loss and the organ index was not different from that of the PBS group. As shown in Figure 7F, H & E staining was utilized to assess the histological alterations in the different groups for different organs, including the hearts, spleens, lungs, kidneys, and brains, and the results showed that there was no significant organ injury in the HNK and the HNK-loaded liposomes; this indicated the safety of Lips/HNK and HA-DOPE@Lips/HNK. In the TUNEL assay (Figure 7G), we could observe stronger green fluorescence of the HA-DOPE@Lips/HNK group than that of other groups. The above results indicated that HA-DOPE@Lips/HNK could act as an ideal nano delivery system to deliver HNK into the OS region and target $CD44^+$ OS cells with less systemic toxicity.

Discussion

Nanotechnology has attracted attention in recent years and is applied in the treatment of OS.[23] Nanoparticles are advantageous because we can achieve the desired drug encapsulation efficiency and increase bioavailability. In addition, nanoparticles can be modified to deliver drugs to the tumor site.[24] HNK is an antitumor drug that is insoluble in water and lacks drug targeting, which restricts its clinical applications.[25] HNK-loaded liposomes combined with HA-DOPE showed good targeting ability to OS cells owing to the interaction between HA and CD44.[26] The cell uptake assay revealed that the uptake efficiency of HA-DOPE@Lips/HNK was significantly higher than that of Lips/HNK, indicating that the targeting ability of HA-DOPE@Lips/HNK to OS cells mainly depended on the modification of HA-DOPE. HNK can effectively induce apoptosis in many tumor cells. For example, HNK induced apoptosis in the Saos-2 and MG63 cells.[27] Also, HA-DOPE@Lips/HNK significantly increased apoptosis compared with HNK and Lips/HNK because it was more up-taken by 143B cells. The cell cycle assay revealed that HNK, Lips/HNK, and HA-DOPE @Lips/HNK could induce G1/M cell arrest. Previous studies have shown that HNK induced 143B cell cycle arrest via the p53/p21 signaling pathway.[28,29] The mitochondrial activity assay revealed that HNK, Lips/HNK, and HA-DOPE @Lips/HNK disrupted the mitochondrial activity, which indicated that HNK can directly target mitochondrial bioenergetics, leading to a persistent inhibition of mitochondrial respiration.[30,31] The biodistribution assay revealed that Lips/DiD and HA-DOPE@Lips/DiD were more accumulated in the liver, lung and spleen, which HA-DOPE@Lips/DiD accumulated in the tumor site. These results indicated that HA-DOPE@Lips/DiD can deliver the drug into the tumor owing to the interaction between HA and CD44. HA and alendronate-modified nanoparticles can deliver curcumin to the OS site.[17] What's more, the HA-coated liposomes could deliver paclitaxel and target tumors and enhance the anti-tumor efficiency in 4T1 tumor-bearing mice.[32] HNK inhibited solid tumor growth and induced apoptosis in vivo. HNK induced apoptosis in HOS and U2OS cells and suppressed tumor growth in the mouse xenograft model.[33] HA-DOPE@Lips/HNK demonstrated superior antitumor efficiency, which may be related to the enhanced tumor targeting of HA. In addition, HNK, Lips/HNK, and HA-DOPE@Lips/HNK have good biocompatibility with no apparent damage to the major organs. In conclusion, our study indicated that HA-DOPE@Lips/HNK is a safe and efficient vehicle for the delivery of HNK to treat OS.

Conclusion

In the present study, we synthesized a targeting delivery system with HA-DOPE@Lips/HNK liposomes for the physical encapsulation of HNK. HA-DOPE@Lips/HNK showed excellent performance with suitable particle size, good stability, high encapsulation rate, and high binding affinity with CD44 of the OS cells. HA-DOPE@Lips/HNK delivered more HNK into OS cells, which greatly improved the in vivo antitumor activity with no obvious organ toxicity. Thus, HA-DOPE@Lips/HNK could be useful for OS applications. This study provided an HNK delivery strategy for the targeted therapy of OS.

Acknowledgments

This work was supported by the Xinglin young scholar construction of high levels university projects of Guangzhou University of Chinese Medicine (A1-2601-21-414-001Z22, A1-AFD018201Z0352 and A1-AFD018191Z0161). We also acknowledge the Lingnan Medical Research Center of Guangzhou University of Chinese Medicine and State Key Laboratory of Biocontrol of Sun Yat-sen University for the support on facilities.

Disclosure

The authors report no conflicts of interest in this work.

References

1. Longhi A, Errani C, De Paolis M, Mercuri M, Bacci G. Primary bone osteosarcoma in the pediatric age: state of the art. *Cancer Treat Rev*. 2006;32(6):423–436. doi:10.1016/j.ctrv.2006.05.005
2. Arndt CA, Rose PS, Folpe AL, Laack NN. Common musculoskeletal tumors of childhood and adolescence. *Mayo Clin Proc*. 2012;87(5):475–487. doi:10.1016/j.mayocp.2012.01.015
3. Chen B, Yang JZ, Wang LF, Zhang YJ, Lin XJ. Ifosfamide-loaded poly (lactic-co-glycolic acid) PLGA-dextran polymeric nanoparticles to improve the antitumor efficacy in osteosarcoma. *BMC Cancer*. 2015;15:752. doi:10.1186/s12885-015-1735-6
4. Isakoff MS, Bielack SS, Meltzer P, Gorlick R. Osteosarcoma: current treatment and a collaborative pathway to success. *J Clin Oncol*. 2015;33(27):3029–3035. doi:10.1200/JCO.2014.59.4895
5. Miwa S, Shirai T, Yamamoto N, et al. Current and emerging targets in immunotherapy for osteosarcoma. *J Oncol*. 2019;2019:7035045. doi:10.1155/2019/7035045
6. Posthuma de Boer J, Royen BJ, Helder M. Mechanisms of therapy resistance in osteosarcoma: a review. *Oncol Discov*. 2013;1(8). doi:10.7243/2052-6199-1-4
7. Alfarouk KO, Stock CM, Taylor S, et al. Resistance to cancer chemotherapy: failure in drug response from ADME to P-gp. *Cancer Cell Int*. 2015;15:71. doi:10.1186/s12935-015-0221-1
8. Luetke A, Meyers PA, Lewis I, Juergens H. Osteosarcoma treatment - where do we stand? A state of the art review. *Cancer Treat Rev*. 2014;40(4):523–532. doi:10.1016/j.ctrv.2013.11.006
9. Afzali D, Sargazi G. Novel uranyl-curcumin-MOF photocatalysts with highly performance photocatalytic activity toward the degradation of phenol red from aqueous solution: effective synthesis route, design and a controllable systematic study. *J Mater Sci Mater Electronics*. 2018;29:18600–18613 doi:10.1007/s10854-018-9978-z.
10. Khan S, Ullah MW, Siddique R, et al. Catechins-modified selenium-doped hydroxyapatite nanomaterials for improved osteosarcoma therapy through generation of reactive oxygen species. *Front Oncol*. 2019;9:499. doi:10.3389/fonc.2019.00499
11. Wang SY, Hu HZ, Qing XC, Zhang ZC, Shao ZW. Recent advances of drug delivery nanocarriers in osteosarcoma treatment. *J Cancer*. 2020;11(1):69–82. doi:10.7150/jca.36588
12. Cichy J, Pure E. The liberation of CD44. *J Cell Biol*. 2003;161(5):839–843. doi:10.1083/jcb.200302098
13. Arpicco S, De Rosa G, Fattal E. Lipid-based nanovectors for targeting of CD44-overexpressing tumor cells. *J Drug Deliv*. 2013;2013:860780. doi:10.1155/2013/860780
14. Kuo JW. *Practical Aspects of Hyaluronan Based Medical Products* . CRC Press. 2005;1217.;1217.
15. Ghosh SC, Neslihan Alpay S, Klostergaard J. CD44: a validated target for improved delivery of cancer therapeutics. *Expert Opin Ther Targets*. 2012;16(7):635–650. doi:10.1517/14728222.2012.687374
16. Coradini D, Pellizzaro C, Miglierini G, Daidone MG, Perbellini A. Hyaluronic acid as drug delivery for sodium butyrate: improvement of the anti-proliferative activity on a breast-cancer cell line. *Int J Cancer*. 1999;81(3):411–416. doi:10.1002/(SICI)1097-0215(19990505)81:3<411::AID-IJC15>3.0.CO;2-F
17. Xi Y, Jiang T, Yu Y, et al. Dual targeting curcumin loaded alendronate-hyaluronan- octadecanoic acid micelles for improving osteosarcoma therapy. *Int J Nanomedicine*. 2019;14:6425–6437. doi:10.2147/IJN.S211981
18. Fried LE, Arbiser JL. Honokiol, a multifunctional antiangiogenic and antitumor agent. *Antioxid Redox Signal*. 2009;11(5):1139–1148. doi:10.1089/ars.2009.2440
19. Haggag YA, Ibrahim RR, Hafiz AA. Design, formulation and in vivo evaluation of novel honokiol-loaded PEGylated PLGA nanocapsules for treatment of breast cancer. *Int J Nanomedicine*. 2020;15:1625–1642. doi:10.2147/IJN.S241428
20. Lin HL, Cheng WT, Chen LC, Ho HO, Lin SY, Hsieh CM. Honokiol/magnolol-loaded self-assembling lecithin-based mixed polymeric micelles (lbMPMs) for improving solubility to enhance oral bioavailability. *Int J Nanomedicine*. 2021;16:651–665. doi:10.2147/IJN.S290444
21. Wu W, Wang L, Wang L, et al. Preparation of honokiol nanoparticles by liquid antisolvent precipitation technique, characterization, pharmacokinetics, and evaluation of inhibitory effect on HepG2 cells. *Int J Nanomedicine*. 2018;13:5469–5483. doi:10.2147/IJN.S178416
22. Zhang Y, Xia Q, Li Y, et al. CD44 assists the topical anti-psoriatic efficacy of curcumin-loaded hyaluronan-modified ethosomes: a new strategy for clustering drug in inflammatory skin. *Theranostics*. 2019;9(1):48–64. doi:10.7150/thno.29715
23. Jia L, Zhang P, Sun H, et al. Optimization of nanoparticles for smart drug delivery: a review. *Nanomaterials*. 2021;11(11):2790. doi:10.3390/nano11112790
24. Singh R, Lillard JW. Nanoparticle-based targeted drug delivery. *Exp Mol Pathol*. 2009;86(3):215–223. doi:10.1016/j.yexmp.2008.12.004
25. Hsiao YP, Chen HT, Liang YC, et al. Development of nanosome-encapsulated honokiol for intravenous therapy against experimental autoimmune encephalomyelitis. *Int J Nanomedicine*. 2020;15:17–29. doi:10.2147/IJN.S214349
26. Surace C, Arpicco S, Dufaÿ-Wojcicki A, et al. Lipoplexes targeting the CD44 hyaluronic acid receptor for efficient transfection of breast cancer cell. *Mol Pharm*. 2009;6:1062–1073. doi:10.1021/mp800215d
27. Yang J, Zou Y, Jiang D. Honokiol suppresses proliferation and induces apoptosis via regulation of the miR21/PTEN/PI3K/AKT signaling pathway in human osteosarcoma cells. *Int J Mol Med*. 2018;41(4):1845–1854. doi:10.3892/ijmm.2018.3433
28. Chio CC, Chen KY, Chang CK, et al. Improved effects of honokiol on temozolomide-induced autophagy and apoptosis of drug-sensitive and -tolerant glioma cells. *BMC Cancer*. 2018;18(1):379. doi:10.1186/s12885-018-4267-z
29. Lin CJ, Chang YA, Lin YL, Liu SH, Chang CK, Chen RM. Preclinical effects of honokiol on treating glioblastoma multiforme via G1 phase arrest and cell apoptosis. *Phytomedicine*. 2016;23(5):517–527. doi:10.1016/j.phymed.2016.02.021
30. Pan J, Lee Y, Cheng G, et al. Mitochondria-targeted honokiol confers a striking inhibitory effect on lung cancer via inhibiting complex I activity. *iScience*. 2018;3:192–207. doi:10.1016/j.isci.2018.04.013

31. Pan J, Lee Y, Wang Y, You M. Honokiol targets mitochondria to halt cancer progression and metastasis. *Mol Nutr Food Res*. 2016;60 (6):1383–1395. doi:10.1002/mnfr.201501007
32. Ravar F, Saadat E, Gholami M, et al. Hyaluronic acid-coated liposomes for targeted delivery of paclitaxel, in-vitro characterization and in-vivo evaluation. *J Control Release*. 2016;229:10–22. doi:10.1016/j.jconrel.2016.03.012
33. Huang K, Chen Y, Zhang R, et al. Honokiol induces apoptosis and autophagy via the ROS/ERK1/2 signaling pathway in human osteosarcoma cells in vitro and in vivo. *Cell Death Dis*. 2018;9(2):157. doi:10.1038/s41419-017-0166-5